Selective Object Rearrangement in Clutter

Anonymous Author(s)
Affiliation
Address
`email`

Abstract: We propose an image-based, learned method for selective tabletop object rearrangement in clutter using a parallel jaw gripper. Our method consists of three stages: graph-based object sequencing (which object to move), feature-based action selection (whether to push or grasp, and at what position and orientation) and a visual correspondence-based placement policy (where to place a grasped object). Experiments show that this decomposition works well in challenging settings requiring the robot to begin with an initially cluttered scene, selecting only the objects that need to be rearranged while discarding others, and dealing with cases where the goal location for an object is already occupied – making it the *first* system to address all these *concurrently* in a purely image-based setting. We also achieve an ∼8% improvement in task success rate over the previously best reported result that handles *both* translation and orientation in less restrictive (uncluttered, non-selective) settings. We demonstrate zero-shot transfer of our system solely trained in simulation to a real robot selectively rearranging up to 15 everyday objects, many unseen during learning, on a crowded tabletop. Videos: `https://sites.google.com/view/selective-rearrangement`.

Keywords: Rearrangement, Robot Manipulation, Task and Motion Planning

1 Introduction

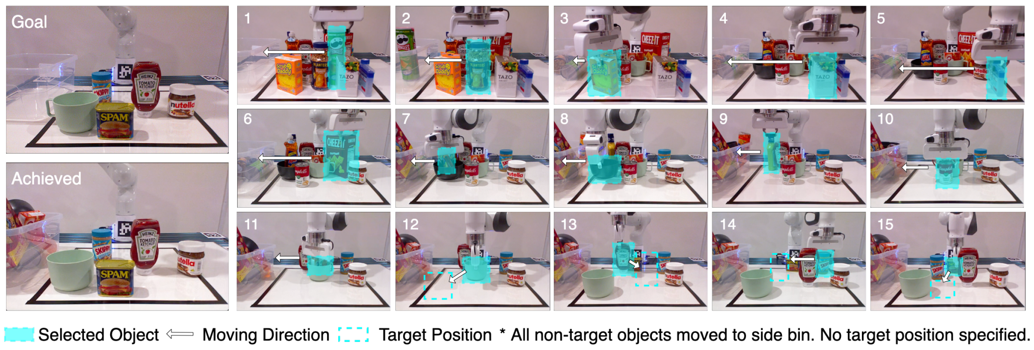

Figure 1: **15-object selective rearrangement from a cluttered initial state.** Given an initial arrangement of everyday objects and an image specifying the goal arrangement, the robot learns to remove objects that do not need repositioning (1-11) and repositions all other objects accurately (12-15) as specified by the goal image (top left) resulting in the final arrangement (bottom left).

Repositioning objects to a desired configuration is rooted in the activities of daily living [1]. Many skills underlie this capability – extracting useful information from raw perceptual data, performing accurate object manipulation, and optimizing long-term sequential action planning – making object rearrangement an essential challenge for both robotics and embodied AI [2]. Figure 1 illustrates our setting: faced with a tabletop with many everyday objects (**clutter**) the robot is tasked to rearrange a subset of objects (**selectivity**) to a goal configuration, while discarding others in a bin. Another challenge is in situations where the desired locations for some objects are already occupied (**swap**). Object rearrangement has been studied in the context of both task and motion planning and learning. However, existing methods do not *concurrently* address these three challenges. Our system is the first to do so in a purely learned setting where the goal is given by a single RGB-D image.

In contrast to e.g., suction mechanisms, we work with a parallel jaw gripper requiring object singulation before grasping. Our method consists of three stages: graph-based **object sequencing** that picks the next object to manipulate by minimizing the Graph Edit Distance (GED) between the current scene graph and the goal scene graph, feature-based **action selection** that maps the RGB-D image to robot actions (pushing or grasping) through a deep Q-learning framework and a visual correspondence-based **placement policy** that uses the cross-correlation of visual features extracted by a pretrained network between the grasped object and the goal specification image to locate object placement. Experiments show that the system successfully rearranges 3-7 objects with higher than 90% completion within 2.99 cm error, and rearranges 16-20 objects with higher than 82.33% success within 1.64 cm error. We also achieve an $\sim$8% improvement in task success rate over the previously best reported result that handles *both* translation and orientation in a less restrictive setting (uncluttered, non-selective). We demonstrate zero-shot transfer to a real robot (Figure 1) selectively rearranging up to 15 everyday objects, many unseen during learning, on a crowded tabletop.

2 Related Work

Task and motion planning-based systems (TAMP) [3] either have a high-level task planner and a low-level motion planner [4, 5, 6, 7, 8, 9, 10], or use sampling-based algorithms or optimization to solve a single unified formulation of the problem [11, 12]. Some TAMP solutions rely on known object models or a known environment [13, 9, 10], which makes it difficult to deploy them with novel objects or where explicit object pose estimation is difficult to obtain. TAMP approaches that incorporate learning-based vision models, such as [14, 15, 16, 17] can adapt to novel objects/environments while [14] is based on one initial scene image, [15] uses structural constrained predicates for planning, [16] depends on the knowledge of the environment, and [17] assumes round collision radius for all object shapes, making it difficult to scale to adversarial environments (e.g., highly cluttered). The number of possible action sequences increases exponentially with the number of objects and changes in environment observability increase the difficulty of back-tracking and replanning.

Deep learning-based systems have relaxed some of these constraints by incorporating learning-based models in perception, planning and actuation. They have been shown to learn general policies to handle varied rearrangement tasks [27, 28, 29, 30, 31, 32, 33], e.g., highly-cluttered, partially-observable environments or deformable objects. Our work is related to learning-based methods for grasping in clutter [18, 19, 20], target object retrieval [21, 22, 23], and rearrangement [24, 25, 10, 26] (Table 1). Most related to our work, Zeng et al. [20] proposed using deep Q-learning to learn synergies between push and grasp actions in order to improve grasping accuracy in densely cluttered environment. Inspired by [20], we adapt collaborative PUSH and GRASP in our system in order to deal with highly cluttered environments for object rearrangement tasks. Different from previous works, we learn action primitives, distinguish objects to rearrange from those to discard, and plan sequential actions simultaneously making this the first work to concurrently solve image-based selective object rearrangement in a cluttered tabletop environment.

Method	Robot Action	Clutter	Selectivity
Grasping			
DexNet [18]	GRASP	✔	✗
GPD [19]	GRASP	✔	✗
VPG [20]	PUSH&GRASP	✔	✗
Target object retrieval			
Mech Search [21]	GRASP	✔	✔
Murali et al. [22]	GRASP	✔	✔
MORE [23]	PUSH&GRASP	✔	✔
Rearrangement			
NeRP [24]	GRASP	✗	✗
IFOR [25]	GRASP	✗	✗
TRLB [10]	SUCTION	✔	✗
ReorientBot [26]	SUCTION	✔	✗
Ours	PUSH&GRASP	✔	✔

Table 1: **Related Manipulation Tasks**

3 Learning a Selective Rearrangement Policy

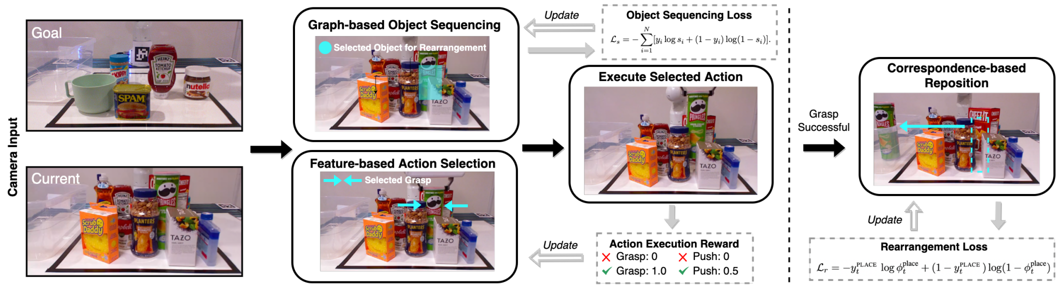
Camera Input
Goal
Current
Graph-based Object Sequencing
Selected Object for Rearrangement
Feature-based Action Selection
Selected Grasp
Update
Object Sequencing Loss
$\mathcal{L}_s = -\sum_{i=1}^{N}[y_i \log s_i + (1-y_i)\log(1-s_i)].$
Execute Selected Action
Action Execution Reward
✗ Grasp: 0 ✗ Push: 0
✓ Grasp: 1.0 ✓ Push: 0.5
Update
Grasp Successful
Correspondence-based Reposition
Update
Rearrangement Loss
$\mathcal{L}_r = -y_t^{\text{PLACE}} \log \phi_t^{\text{place}} + (1-y_t^{\text{PLACE}})\log(1-\phi_t^{\text{place}})$

Figure 2: **System overview.** Our system uses RGB-D images as input and builds a scene graph based on the object segmentation given by UOIS-Net-3D [34]. Graph-based object sequencing (subsection 3.3) selects the optimal object for next rearrangement and we mask the Q-value map for GRASP with its segmentation mask. Then the system picks the highest Q-value action candidate from PUSH and GRASP Q-value maps and executes the action Figure 3a. If GRASP is chosen and successfully executed, the system locates the PLACE of the grasped object (Figure 3b).

We decompose the rearrangement problem into three parts: object sequencing (*which* object to relocate next), action selection (*how* to manipulate it), and object placement (*where* to place a grasped object). We rely on three primitives: pushing objects (PUSH), picking them up (GRASP), and placing them at the target locations (PLACE). PUSH and GRASP can be initiated by the robot at any time, however PLACE can only be performed if the robot is already holding an object. This suggests a natural decomposition into our three part strategy. When the robot is not holding an object, it must make a decision on which object to manipulate next (object sequencing). After choosing an object, it must decide whether (and how) to push the selected object or whether (and how) to pick it up (action selection). When holding an object, it must decide where to place it (object placement). We model object sequencing as a supervised learning problem on graph transformations (subsection 3.3), action selection as a Partially Observable Markov Decision Process (POMDP) (subsection 3.1), and object placement as a supervised learning problem (subsection 3.2).

3.1 Feature-based Action Selection: PUSH or GRASP

The choice of whether to PUSH or GRASP (and at what location and orientation to execute these actions) is Markovian since it is based solely on the current state (object poses). Further, the state is partially observable – we do not assume the robot has direct access to full state information, it needs to be inferred from images. Hence, we formulate the problem of selecting whether to push or pick up an object (and at what location and orientation) as a goal-conditioned POMDP.

A goal-conditioned POMDP is a tuple $(\mathcal{S}, \mathcal{G}, \mathcal{A}, p, \mathcal{R}, \Omega, \mathcal{O}, \gamma, \rho_0, \rho_g)$ where $\mathcal{S}$ is the state space, $\mathcal{G}$ is the set of goals, $\mathcal{A}$ is the action space, $p(\mathbf{s_{t+1}}|\mathbf{s_t}, \mathbf{a_t})$ is the time-invariant (unknown) dynamics function, $R : S \times A \rightarrow \mathbb{R}$ is the reward function, Ω is a set of observations, O is a set of conditional observation probabilities, $\gamma \in [0, 1]$ is the discount factor, ρ_0 is the initial state distribution, and ρ_g is the goal distribution. The objective in goal-conditioned reinforcement learning is to obtain a policy $\pi(\mathbf{a_t}|\mathbf{s_t}, \mathbf{g})$ to maximize the expected sum of rewards $\mathbb{E}[\sum_t R(\mathbf{s_t}, \mathbf{g})]$, where the goal is sampled from ρ_g and the states are sampled according to $\mathbf{s_0} \sim \rho_0$, and $\mathbf{s_{t+1}} \sim \mathbf{p}(\mathbf{s_{t+1}}|\mathbf{s_t}, \mathbf{a_t})$.

We define the state s as the poses of N objects in the scene. The actions $a \in A$ consist of the choice of action ψ, end-effector position x and planar orientation θ: $a = (\psi, x, \theta), \psi \in \{\text{PUSH}, \text{GRASP}\}, x \in \mathbb{R}^3, \theta \in \mathbb{R}$. We choose a sparse reward for actions - 1.0 for successful GRASP and 0.5 for successful PUSH. The higher reward for GRASP incentivizes the robot to prioritize it over PUSH when both are available. We consider a PUSH successful if the pixel-wise change in the depth image after a PUSH is larger than a pre-defined threshold. The intuition behind designing the PUSH reward this way is that we only use it for singulating objects in clutter where direct GRASP is not available, not for object rearrangement. A GRASP is considered successful if the antipodal distance between the parallel-jaw gripper fingers after a GRASP attempt is higher than a pre-defined thresh-

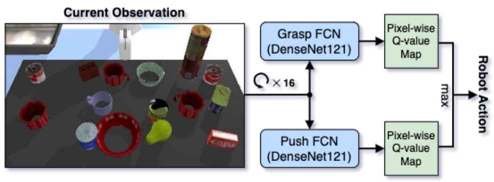

(a) Feature-based Action Selection

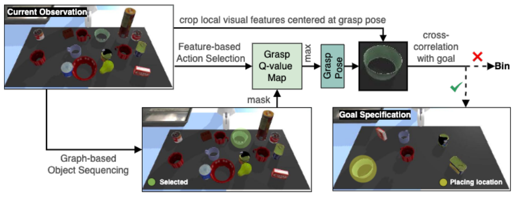
Current Observation
crop local visual features centered at grasp pose
Feature-based Action Selection
Grasp Q-value Map
max
Grasp Pose
cross-correlation with goal
Bin
mask
Graph-based Object Sequencing
Selected
Goal Specification
Placing location

(b) Correspondence-based Reposition

Figure 3: **Subpolicies.** (a) A deep Q-learning framework maps the visual observations to actions, similar to [20]. (b) The grasped object placement is conditioned on the cross-correlation between the visual feature of the goal scene and the local features of the grasped object.

old. Observation o_t is defined as the RGB-D image captured by a statically mounted camera. The goal specification o_g is the RGB-D image of the goal arrangement from the same camera viewpoint.

Given the current observation o_t we use fully convolutional neural networks (FCNs) to model Q-functions that estimate the expected reward for each PUSH and GRASP candidate. The deep Q-learning framework is shown in Figure 3a. A 121-layer DenseNet [35] pretrained on ImageNet [36] is used to extract visual features from raw RGB-D images. In each FCN, we have three 1×1 convolutional layers; we apply batch normalization and ReLU activation before every convolutional layer. After FCN, we upsample with bilinear mode to have a pixel-wise Q-value estimate of the same size as input images. Each pixel unit in the Q-value map corresponds to the expected reward for executing an action at this pixel location. For each action we model end-effector orientation by rotating o_t to 16 different orientations. Thus we have 32 pixel-wise Q-value maps (16 each for PUSH and GRASP). Each represents the Q-value estimate of executing the corresponding action at that orientation at all pixel locations. At each timestep t, before the robot chooses the next action, we mask all 16 GRASP Q-value maps with the output from the graph-based object rearrangement sequencing module (Figure 3b) to rule out objects that do not currently need to be repositioned. Following this, the robot picks an action (PUSH or GRASP) with the highest Q-value and executes it at the corresponding pixel location and end-effector orientation.

Loss is calculated by computing the temporal difference (TD) between the estimated reward and the actual obtained reward after execution. We only compute the loss for the selected pixel/pose (where the robot will take the next action); all other pixels/poses backpropagate with loss 0. We generate the label for PUSH at time t, y_t^{PUSH}, by calculating the depth image change after the push – if it is higher than a predefined threshold we consider the PUSH successful, $y_t^{\text{PUSH}} = 0.5$. For GRASP, we obtain the label at time t, y_t^{GRASP}, via the feedback signal from the gripper, if the antipodal distance between parallel jaws is larger than a predefined threshold, we consider the gripper is holding the object and hence the GRASP is successful, $y_t^{\text{GRASP}} = 1$. We use a Huber Loss for both PUSH and GRASP. For action executed at time t, let y_t denote the label, Q_t denote the estimated reward. The TD is given by $|Q_t - y_t|$, and the primitive learning loss is calculated as:

$$\mathcal{L}_p = \begin{cases} \frac{1}{2}(Q_t - y_t)^2, & |Q_t - y_t| < 1, \\ |Q_t - y_t| - \frac{1}{2}, & \text{otherwise.} \end{cases}$$

3.2 Correspondence-based Reposition: Where to PLACE

We model finding PLACE pose at time t as a template matching problem [37] conditioned on the current observation o_t, the goal specification o_g, and the successfully executed GRASP τ_{t-1} at time $t-1$. We use a pretrained ResNet [38] to extract visual feature maps for both o_t and o_g. Let $\phi(o_t)$ denote the visual feature map for o_t. Given the executed GRASP $\tau_{t-1} = (x_{t-1}, \theta_{t-1})$, where x_{t-1} represents the GRASP location and θ_{t-1} represents the end-effector rotation, we crop a visual feature segment $\phi(o_{t-1})[\tau_{t-1}]$ with a predefined crop window size centered at x_{t-1}, and we consider $\phi(o_{t-1})[\tau_{t-1}]$ as a template for the grasped object (Figure 3b). The cross-correlation between $\phi(o_{t-1})[\tau_{t-1}]$ and $\phi(o_g)$ outputs a similarity distribution showing the resemblance between

$\phi(o_{t-1})[\tau_{t-1}]$ and the local features at every placement in $\phi(o_g)$:

$$\varphi_t^{\text{similarity}} = \phi(o_{t-1})[\tau_{t-1}] * \phi(o_g).$$

Different from [37], we also apply cross-correlation between depth images o_g^{depth} and o_t^{depth}: $\varphi_t^{\text{depth}} = \phi(o_t^{\text{depth}}) * \phi(o_g^{\text{depth}})$, which outputs a pixel-wise distribution over the workspace indicating whether a pixel location is occupied by objects in the current scene or in the goal scene. The prediction for PLACE is given by: $\varphi_t^{\text{PLACE}} = \varphi_t^{\text{similarity}} - \varphi_t^{\text{depth}}$. By lowering the value for occupied pixels we avoid placing the grasped object on top of other objects or at goal positions of other objects. φ_t^{PLACE} is a pixel-wise prediction and each pixel represents a potential placement for the grasped object; to model the end-effector rotation of PLACE, we rotate the current image o_t to 16 different orientations as input and pick the one with the highest prediction value. The non-occupied location in $\phi(o_g)$ with the highest cross-correlation value is considered as the best PLACE τ_t^{place} for the grasped object. If a match cannot be found in o_g, i.e. the similarity score is below a predefined threshold for all pixel locations, the object is placed aside in the bin. The training loss for PLACE policy learning is cross-entropy. The ground-truth goal position and orientation of the grasped object are extracted directly from the simulator. We generate the label y_t^{PLACE} by assigning value 1 to the pixel at the goal location of the grasped object; all other pixels are set to 0. The learning objective is to maximize the visual feature extraction model's prediction accuracy given a goal image and a template. While we rotate the input image in 16 different directions to differentiate placing orientations, only assign value 1 for the one with correct goal orientation. The rearrangement loss is calculated as:

$$\mathcal{L}_r = -y_t^{\text{PLACE}} \log \phi_t^{\text{PLACE}} + (1 - y_t^{\text{PLACE}}) \log(1 - \phi_t^{\text{PLACE}}).$$

3.3 Graph-based Object Sequencing: Which Object is Next

Graph Generation We construct an accessibility graph representing reachable traversal paths from the robot end-effector location to every object. Unlike [39] (which assumes a known geometry for all objects and uses the graph for target object retrieval tasks), we use UOIS-Net-3D [34] to provide a set of object segmentation masks from raw RGB-D images. We consider each segmented object as a vertex $v \in \mathcal{V}$ in the scene graph and add v_r as the robot vertex. An edge $e \in \mathcal{E}$ between a pair of vertices means a collision-free end-effector path exists between them. The graph generation algorithm is shown in algorithm 1. Examples of generated scene graphs are shown in the supplement. The traversal path from the robot vertex to any object vertex in the generated scene graph captures the shortest path from the robot base to any object in the workspace, which includes objects that are blocking the straight line path.

Algorithm 1: ACC-GRAPH GENERATION

```
Input: camera observation $\mathcal{O}$ of a scene.
Output: accessibility graph $\mathcal{G} = (\mathcal{V}, \mathcal{E})$.
1  $\mathcal{E} \leftarrow \varnothing, \mathcal{V} \leftarrow \varnothing, \mathcal{V}' \leftarrow \varnothing$
2  Get segmentation from UOIS-Net-3D($\mathcal{O}$)
3  Each segmented object maps to $v \in \mathcal{V}'$
4  Create robot vertex $v_r$, $\mathcal{V} \leftarrow \{v_r\}$
5  while $\exists v \in \mathcal{V}'$ and $v \notin \mathcal{V}$ do
6      for every $v_i \in \mathcal{V}$ do
7          for every $v_j \in \mathcal{V}'$ do
8              if linear distance path $(v_i, v_j)$ is collision-free then
9                  $\mathcal{E} \leftarrow \mathcal{E} \cup \{(v_i, v_j)\}$
10                 $\mathcal{V} \leftarrow \mathcal{V} \cup \{v_j\}$
11                 $\mathcal{V}' \leftarrow \mathcal{V}' - \{v_j\}$
12 return $\mathcal{G} = (\mathcal{V}, \mathcal{E})$
```

Object Sequencing Let o_t and o_g denote the current and the goal scenes, and $\mathcal{G}_t$, $\mathcal{G}_g$ denote the current and the goal scene graphs. We establish a list of sub-graphs of $\mathcal{G}_t$ by individually removing each vertex and its related edges. We calculate the similarity between each sub-graph and the goal graph through a pretrained SimGNN [40], previously shown to be an excellent approximator ($MSE < 1.18 \times 10^{-3}$). The graph similarity corresponds to the Graph Edit Distance (GED) between two graphs G_1 and G_2 – the number of edit operations in the optimal alignment that transform

Algorithm 2: OBJECT REARRANGEMENT SEQUENCING

```
Input: accessibility graphs of the current and the goal scene, $\mathcal{G}_t = (\mathcal{V}_t, \mathcal{E}_t)$ and $\mathcal{G}_g = (\mathcal{V}_g, \mathcal{E}_g)$.
Output: selected object $v \in \mathcal{G}_t$ for next rearrangement.
1  $n \leftarrow \mathcal{V}_t.size$
2  Initialize an array sim$[1, ..., n] \leftarrow 0$
3  for every $v_i \in \mathcal{V}_t$ do
4      $\mathcal{G}_t^i \leftarrow \mathcal{G}_t - \{v_i\}$
5      sim[i] $\leftarrow$ Sim_GNN($\mathcal{G}_t^i$, $\mathcal{G}_g$)
6  selected $\leftarrow \arg\max$ sim$[1, ..., n]$
7  return $\mathcal{V}_t$[selected]
```

G_1 into G_2, where an edit operation on a graph is an insertion or deletion of a vertex/edge or relabelling of a vertex (two isomorphic graphs have GED of 0). The removed vertex, i.e. object, from the highest similarity sub-graph is selected to be rearranged next. The robot thus chooses the object responsible for the largest difference between the current scene graph and the goal scene graph, to keep the number of actions towards task completion as low as possible. We show the process of choosing next object to rearrange in algorithm 2.

Loss Calculation We use A^* to calculate the ground-truth GED between graphs [41], since the generated scene graphs are relatively small. To lay the foundation for scaling up to more complex scene graphs in the future (where the ground-truth GED might be inaccessible or computationally expensive to obtain) we use SimGNN to approximate GED for all scene graphs instead of using the ground-truth GED directly. We transform the ground-truth GED between G_1 and G_2 to ground-truth similarity labels y in the range $(0, 1]$ [40]:

$$y = e^{-\text{Norm\_GED}(G_1,G_2)} \qquad \text{Norm\_GED}(G_1, G_2) = \frac{\text{GED}(G_1, G_2)}{(|G_1| + |G_2|)/2}$$

where $|G|$ denotes the number of vertices in G. Let s_i denote the similarity prediction output between $\mathcal{G}_t^i$ and $\mathcal{G}_g$ from SimGNN and $y_i, i = 1, ..., N$ denote the ground-truth similarity label. We use the cross-entropy loss for the graph-based object rearrangement sequencing:

$$\mathcal{L}_s = -\sum_{i=1}^{N}[y_i \log s_i + (1 - y_i) \log(1 - s_i)].$$

After selecting an object for rearrangement, its placement is located as described in subsection 3.2.

4 Evaluation

4.1 Experimental Results in Simulation

We use a position controlled Franka Panda arm with a parallel-jaw gripper in Pybullet [42]. A simulated RealSense D415 RGB-D camera with resolution 640 × 480 is statically mounted. A side bin is placed to hold objects removed from the workspace.

Method	Rotation	Swap	Clutter	Selectivity	Init. #obj.	Goal #obj.	Completion ↑	Position Error ↓
NeRP [24]	✗	✓	✗	✗	3-8	3-8	94.56 ± 0.73	1.90 ± 1.30
IFOR [25]	✓	✓	✗	✗	1-9	1-9	81.80	2.70 ± 2.30
Ours	✓	✗	✗	✗	3-7	3-7	96.67 ± 1.67	1.29 ± 0.91
Ours	✓	✓	✗	✗	3-7	3-7	90.00 ± 3.00	2.99 ± 2.37
Ours	✓	✗	✗	✓	3-7	1-5	97.33 ± 0.67	1.41 ± 2.70
Ours	✓	✓	✗	✓	3-7	1-5	97.00 ± 1.00	1.81 ± 2.66
Ours	✓	✗	✓	✓	16-20	5-10	85.67 ± 2.33	1.64 ± 0.44
Ours	✓	✓	✓	✓	16-20	5-10	82.33 ± 2.67	1.22 ± 0.93

Table 2: **Task Completion (mean %) and Position Error** $(10^{-2}m)$**.** Init./Goal #obj. indicates the number of objects in the initial/goal scene respectively. NeRP [24] and IFOR [25] are state-of-the-art models for image-based tabletop rearrangement. Statistics on both models quoted here are as reported in their original paper (codebases are not publicly available). NeRP is restricted to translation in object repositioning. Since we handle both translation and rotation we compare with IFOR. We achieve a higher task completion (90%) than IFOR (81.8%) in the same setting (reduced clutter, no selectivity, but swaps may be needed since some target locations are occupied). We also handle significantly more complex cases than either of the previous models (e.g., last row of the table shows concurrent challenges handled by our system: high clutter, selectivity, with swaps needed).

We conduct 6 sets of simulation experiments (each with 3 random seeds and 100 episodes) with different variations as shown in Table 2. In each episode, we randomly pick $3 \leq N \leq 20$ objects from the YCB dataset [43] and select a subset of the chosen objects to rearrange on the table. Note that it is possible to choose all N objects for rearrangement or some subset. Objects to be rearranged

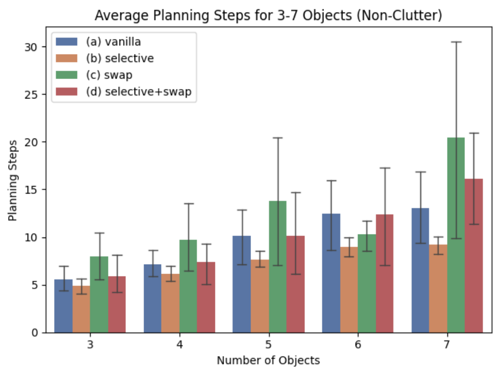

(a) 3-7 objects

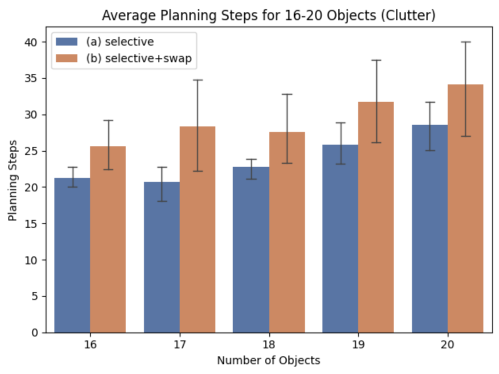

(b) 16-20 objects

Figure 4: **Average Planning Steps** Tasks with target selection require fewer planning steps, introducing swap actions in the task setting increases planning steps. The number of planning steps increases as the number of objects in the scene grows.

are placed at random goal positions and orientations and an RGB-D image is captured. This image is the goal specification. Next, we randomly reposition and rotate all these objects and add the remaining objects (those not designated for rearrangement) at randomly generated positions and orientations to the workspace. The resulting scene is the initial state of the episode.

We add objects in test episodes that the robot had not seen in the training episodes to show the system's adaptability to novel objects. We differentiate the difficulty of rearrangement tasks by measuring the degree to which the scene is cluttered, the degree of selectivity (how many of the objects are designated for rearrangement), and how many swap actions are needed. **(1) Clutter** Let $\mathbf{P} = \{(x_1, y_1), ..., (x_n, y_n)\}$ denote object positions. We define a clutter coefficient:

$$c(\mathbf{P}) = -\log\{\frac{1}{n}\sum_{i}^{n}\sqrt{(x_i - \hat{x_i})^2 + (y_i - \hat{y_i})^2}\}, \quad \hat{x_i} = \mathbf{kNN}(\mathbf{y}), \hat{y_i} = \mathbf{kNN}(\mathbf{x}),$$

in which $\mathbf{kNN}(\mathbf{y}), \mathbf{kNN}(\mathbf{x})$ estimates $\hat{x_i}, \hat{y_i}$ through k-nearest neighbor regression on every other object's position. We consider arrangements with $c(\mathbf{P}) \geq 1.0$ as 'cluttered'. Example scenes and clutter calculations are in the supplement Appendix A. **(2) Selectivity** In selective episodes, only a proper subset of objects in the initial arrangement is included in the goal arrangement. Hence, the system needs to identify which objects are designated to remain on the table before manipulating them. **(3) Swap** Some episodes require swap actions, where the goal positions of certain objects are occupied by other objects in the initial arrangement. This requires the robot to first move the blocking object and then reposition the original object to be rearranged.

We evaluate our method with three metrics: **(1) Task completion** is the percentage of completion in all rearrangement episodes. We consider an episode to be complete when all target objects are placed within 5 cm from their goal position (consistent with prior work [25]) and all non-target objects are placed in the side bin. **(2) Position error** is the average Euclidean distance between the desired target arrangement and the final arrangement achieved. **(3) Planning steps** is defined as the average number of actions the robot takes in each completed episode. It is a measure of the planning efficiency of the learned rearrangement policy.

Our system performs rearrangement in a variety of settings, generalizing readily from 3-20 objects (Table 2, Figure 4). Task completion is calculated over all test episodes; planning steps and position error are only reported on successful episodes. The task completion rate decreases as the task setting becomes more difficult, the position error is stable across all task settings, which indicates an accurate placement prediction from the sub-policy shown in Figure 3b. In selective episodes, our system has a higher task completion rate than non-selective episodes when other task settings are the same. We ascribe this to the graph-based object sequencing module (subsection 3.3) that prioritizes removing non-target objects over rearranging target objects, thus decreasing the clutter coefficient of the current scene and potentially improving the success rate (see supplement Table 2 for details). The task completion rate decreases in situations with high clutter and swap actions. With increased clutter, it is more difficult to find 'buffer' locations for objects whose goal positions are occupied by other objects or objects that are occupying others' goal locations.

NeRP [24] and IFOR [25] are state-of-the-art models for image-based tabletop rearrangement. Like IFOR, our method includes planar rotation alignment of objects (examples in supplement subsection B.2) while NeRP only considers translations. Thus we compare our results with IFOR and show that we achieve a 8.2% higher task completion rate than IFOR in the same task setting at a comparable rotation error (ours:13.89°, IFOR:13.70°).

In Figure 4, we observe that when the task setting remains the same, the number of planning steps increases as the number of objects increases. When target selection is involved, the number of planning steps decreases, as the object sequencing mechanism prioritizes removing non-target objects from the table, leaves a more sparse arrangement of objects in the workspace, potentially reducing subsequent task difficulty. The introduction of swap actions, however, significantly increases the number of planning steps in each task completion. The swap action requires the robot to sample 'buffer' locations for objects whose goal position is occupied, place objects at 'buffer' locations, remove the 'placeholder' objects at their goal positions and then reposition the objects at their goal locations. This process naturally adds more required actions towards task completion.

Two noteworthy recent rearrangement systems are TRLB [10] and ReorientBot [26]. Both rely on suction mechanisms to manipulate objects in clutter without the need to singulate them. TRLB relies on the initial and goal states being fully specified as object poses with a focus on fast planning for rearrangement and ReorientBot relies on the goal state being fully specified as object poses. Our task is sufficiently different (gripper instead of a suction mechanism, goal specified only by a single image) making a direct comparison between our work and these two systems infeasible.

4.2 Ablation Studies

Target Object Selection: In selective rearrangement, the objects in the goal scene (target objects) might be a subset of those in the initial scene. We evaluate the significance of using ResNet to obtain an accurate visual feature cross-correlation and target object classification by testing 2 different encoder-decoder structured visual feature extractors, ResNet [38] and U-Net [44]. We measure the match success rate, average position prediction error and target object classification accuracy over 100 different initial and goal arrangements. The choice of visual feature extraction model is crucial to our entire system because it directly affects the accuracy of target object identification and reposition. Our experiments show that the chosen visual feature extraction model (ResNet) achieves match success rate of 93.33%, position error within 2.04 cm and target classification accuracy of 98.58% with 1-20 objects. Further details are in subsection B.3 of the supplement.

Graph-based Object Sequencing: To verify the importance of graph-based object sequencing to minimize the number of actions, we test two scene graph generation methods and measure their impact on the average number of planning steps. We also consider the situation when no sequencing mechanism is used (no scene graph) and the robot picks the next object only based on PUSH and GRASP Q-value estimates. We generate the scene graph in two ways; a position-based approach which captures the basic spatial relationships among objects and an accessibility approach (subsection 3.3 algorithm 1). We perform object sequencing (algorithm 2) given the scene graph $\mathcal{G}_t$ and the goal scene graph $\mathcal{G}_g$. Compared with no sequencing, using the accessibility graph decreases planning steps by 55.56% (10-object rearrangement) and by 43.71% (20-object rearrangement).

Scene Graph	10	20
N/A	35.13±3.55	45.22±4.70
Position	19.94±4.93	29.29±3.52
Accessibility	**15.61**±3.84	**25.45**±3.88

Table 3: **Scene Graph Comparisons.** Average planning steps vs. # of objects in the initial scene. All scenarios have 10 target objects.

Compared with the position-based approach, using the accessibility graph decreases planning steps by 21.72% (10-object rearrangement) and by 13.11% (20-object rearrangement) thus confirming the efficacy of graph-based object sequencing. A detailed analysis is in the supplement subsection B.4.

4.3 Demonstration on a Physical Robot

We test our system on a Panda robot arm with a parallel-jaw gripper, and a statically-mounted RGB-D camera overlooking a tabletop to capture an image of the workspace (Figure 5). A bin next to the workspace holds the redundant (non-target) objects. Objects included in the demonstration vary across experiments, including a collection of 20 daily use objects (e.g. peanut butter jar, ketchup bottle). The robot demonstration generalizes to novel objects not available during training. We show zero-shot transfer from simulation to real robot setting in the video.

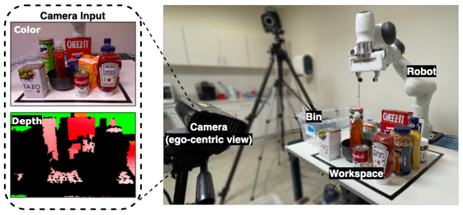

Figure 5: **Robot experiments.**

5 Limitations

Our system has several limitations. **(1) 6 DOF rotation.** Our system is limited to planar object rotations. We do not currently handle 6 DOF object reorientation, and our system is poor at orienting natural objects like oranges and apples which are rotationally symmetric. **(2) Cluttered final state.** Even though our method solves difficult rearrangement tasks with cluttered *initial* object arrangements, it struggles with scenarios where the desired goal arrangement is cluttered. Not surprisingly, this is a significant challenge for other existing systems as well since with a large number of objects it turns into a difficult packing or stacking problem. **(3) Segmenting objects.** Our system is object-centric since we use scene segmentation to build scene graphs and sequence objects. Incorrect object segmentation results in inaccurate object sequencing leading to performance degradation. **(4) Underlying motion planner limitations.** In some experiments, we have experienced difficulties with joint limits being reached when the initial grasp for an object turns out to not be feasible for object placement in the new location or when the robot carrying an object collides with another object. We believe limitations 1,3 and 4 can be addressed respectively by expanding the action space in the action selection module, a better camera (or multiple cameras) and better image segmentation techniques, and better trajectory-aware obstacle-avoiding planners.

6 Conclusions

We proposed an effective image-based learned method for selective tabletop object rearrangement in clutter. Our simulated experiments provide evidence that the method works well in challenging settings which require the robot to begin with an intially cluttered scence, select only the objects that need to be rearranged while discarding others, deal with cases where the target location for an object is already occupied - making the system the first of its kind to be able to address all these concurently. Ablation studies provide an analysis of system performance. We also demonstrate zero-shot transfer of our system to a real robot and generalization to unseen objects.

References

[1] S. Katz. Assessing self-maintenance: activities of daily living, mobility, and instrumental activities of daily living. *Journal of the American Geriatric Society*, 31(12):721–7, 1983.

[2] D. Batra, A. X. Chang, S. Chernova, A. J. Davison, J. Deng, V. Koltun, S. Levine, J. Malik, I. Mordatch, R. Mottaghi, et al. Rearrangement: A challenge for embodied AI. *arXiv preprint arXiv:2011.01975*, 2020.

[3] C. R. Garrett, R. Chitnis, R. Holladay, B. Kim, T. Silver, L. P. Kaelbling, and T. Lozano-Pérez. Integrated task and motion planning. *Annual review of control, robotics, and autonomous systems*, 2021.

[4] A. Krontiris and K. E. Bekris. Dealing with difficult instances of object rearrangement. In *Robotics: Science and Systems*, 2015.

[5] J. E. King, M. Cognetti, and S. S. Srinivasa. Rearrangement planning using object-centric and robot-centric action spaces. In *IEEE Intl. Conf. on Robotics and Automation*, 2016.

[6] S. D. Han, N. M. Stiffler, A. Krontiris, K. E. Bekris, and J. Yu. Complexity results and fast methods for optimal tabletop rearrangement with overhand grasps. *The International Journal of Robotics Research*, 2018.

[7] C. R. Garrett, T. Lozano-Pérez, and L. P. Kaelbling. Pddlstream: Integrating symbolic planners and blackbox samplers via optimistic adaptive planning. In *Proceedings of the Intl. Conf. on Automated Planning and Scheduling*, 2020.

[8] S. H. Cheong, B. Y. Cho, J. Lee, C. Kim, and C. Nam. Where to relocate?: Object rearrangement inside cluttered and confined environments for robotic manipulation. In *IEEE Intl. Conf. on Robotics and Automation*, 2020.

[9] R. Wang, K. Gao, D. Nakhimovich, J. Yu, and K. E. Bekris. Uniform object rearrangement: From complete monotone primitives to efficient non-monotone informed search. In *IEEE Intl. Conf. on Robotics and Automation*, 2021.

[10] K. Gao, D. Lau, B. Huang, K. E. Bekris, and J. Yu. Fast high-quality tabletop rearrangement in bounded workspace. In *IEEE Intl. Conf. on Robotics and Automation*, 2022.

[11] M. Stilman, J.-U. Schamburek, J. Kuffner, and T. Asfour. Manipulation planning among movable obstacles. In *IEEE Intl. Conf. on Robotics and Automation*, 2007.

[12] M. Toussaint. Logic-geometric programming: An optimization-based approach to combined task and motion planning. In *Twenty-Fourth International Joint Conference on Artificial Intelligence*, 2015.

[13] L. P. Kaelbling and T. Lozano-Pérez. Hierarchical task and motion planning in the now. In *IEEE Intl. Conf. on Robotics and Automation*. IEEE, 2011.

[14] D. Driess, J.-S. Ha, and M. Toussaint. Deep visual reasoning: Learning to predict action sequences for task and motion planning from an initial scene image. In *Robotics: Science and System*, 2020.

[15] C. R. Garrett, C. Paxton, T. Lozano-Pérez, L. P. Kaelbling, and D. Fox. Online replanning in belief space for partially observable task and motion problems. In *IEEE Intl. Conf. on Robotics and Automation*, 2020.

[16] B. Ichter, P. Sermanet, and C. Lynch. Broadly-exploring, local-policy trees for long-horizon task planning. *arXiv preprint arXiv:2010.06491*, 2020.

[17] Y. Labbé, S. Zagoruyko, I. Kalevatykh, I. Laptev, J. Carpentier, M. Aubry, and J. Sivic. Monte-carlo tree search for efficient visually guided rearrangement planning. *IEEE Robotics and Automation Letters*, 2020.

[18] J. Mahler, M. Matl, V. Satish, M. Danielczuk, B. DeRose, S. McKinley, and K. Goldberg. Learning ambidextrous robot grasping policies. *Science Robotics*, 2019.

[19] A. ten Pas, M. Gualtieri, K. Saenko, and R. Platt. Grasp pose detection in point clouds. *The International Journal of Robotics Research*, 2017.

[20] A. Zeng, S. Song, S. Welker, J. Lee, A. Rodriguez, and T. Funkhouser. Learning synergies between pushing and grasping with self-supervised deep reinforcement learning. In *IEEE/RSJ Intl. Conf.on Intelligent Robots and Systems*, 2018.

[21] M. Danielczuk, A. Kurenkov, A. Balakrishna, M. Matl, D. Wang, R. Martín-Martín, A. Garg, S. Savarese, and K. Goldberg. Mechanical search: Multi-step retrieval of a target object occluded by clutter. In *IEEE Intl. Conf. on Robotics and Automation*, 2019.

[22] A. Murali, A. Mousavian, C. Eppner, C. Paxton, and D. Fox. 6-dof grasping for target-driven object manipulation in clutter. In *IEEE Intl. Conf. on Robotics and Automation*, 2020.

[23] B. Huang, S. D. Han, J. Yu, and A. Boularias. Visual foresight trees for object retrieval from clutter with nonprehensile rearrangement. *IEEE Robotics and Automation Letters*, 2022.

[24] A. H. Qureshi, A. Mousavian, C. Paxton, M. C. Yip, and D. Fox. Nerp: Neural rearrangement planning for unknown objects. In *Proceedings of Robotics: Science and Systems*, 2021.

[25] A. Goyal, A. Mousavian, C. Paxton, Y.-W. Chao, B. Okorn, J. Deng, and D. Fox. Ifor: Iterative flow minimization for robotic object rearrangement. In *arXiv:2202.00732*, 2022.

[26] K. Wada, S. James, and A. J. Davison. ReorientBot: Learning object reorientation for specific-posed placement. In *IEEE Intl. Conf. on Robotics and Automation*, 2022.

[27] I. Kapelyukh and E. Johns. My house, my rules: Learning tidying preferences with graph neural networks. In *Conference on Robot Learning*, 2022.

[28] D. Seita, P. Florence, J. Tompson, E. Coumans, V. Sindhwani, K. Goldberg, and A. Zeng. Learning to Rearrange Deformable Cables, Fabrics, and Bags with Goal-Conditioned Transporter Networks. In *IEEE Intl. Conf. on Robotics and Automation*, 2021.

[29] H. Ha and S. Song. Flingbot: The unreasonable effectiveness of dynamic manipulation for cloth unfolding. In *Conference on Robot Learning*, 2022.

[30] M. Shridhar, L. Manuelli, and D. Fox. Cliport: What and where pathways for robotic manipulation. In *Conference on Robot Learning*, 2022.

[31] J. Ahn, C. Kim, and C. Nam. Coordination of two robotic manipulators for object retrieval in clutter. *arXiv preprint arXiv:2109.15220*, 2021.

[32] H. Wu, J. Ye, X. Meng, C. Paxton, and G. Chirikjian. Transporters with visual foresight for solving unseen rearrangement tasks. *arXiv preprint arXiv:2202.10765*, 2022.

[33] C. Paxton, C. Xie, T. Hermans, and D. Fox. Predicting stable configurations for semantic placement of novel objects. In *Conference on Robot Learning*, 2022.

[34] C. Xie, Y. Xiang, A. Mousavian, and D. Fox. Unseen object instance segmentation for robotic environments. *IEEE Transactions on Robotics (T-RO)*, 2021.

[35] G. Huang, Z. Liu, L. Van Der Maaten, and K. Q. Weinberger. Densely connected convolutional networks. In *IEEE conference on computer vision and pattern recognition*, 2017.

[36] A. Krizhevsky, I. Sutskever, and G. E. Hinton. Imagenet classification with deep convolutional neural networks. *Advances in neural information processing systems*, 2012.

[37] A. Zeng, P. Florence, J. Tompson, S. Welker, J. Chien, M. Attarian, T. Armstrong, I. Krasin, D. Duong, V. Sindhwani, and J. Lee. Transporter networks: Rearranging the visual world for robotic manipulation. *Conference on Robot Learning*, 2020.

[38] K. He, X. Zhang, S. Ren, and J. Sun. Deep residual learning for image recognition. In *2016 IEEE Conference on Computer Vision and Pattern Recognition (CVPR)*, 2016.

[39] C. Nam, J. Lee, S. Hun Cheong, B. Y. Cho, and C. Kim. Fast and resilient manipulation planning for target retrieval in clutter. In *IEEE Intl. Conf. on Robotics and Automation*, 2020.

[40] Y. Bai, H. Ding, S. Bian, T. Chen, Y. Sun, and W. Wang. SimGNN: A neural network approach to fast graph similarity computation. In *ACM Intl. Conf. on Web Search and Data Mining*, 2019.

[41] K. Riesen, S. Emmenegger, and H. Bunke. A novel software toolkit for graph edit distance computation. In *International Workshop on Graph-Based Representations in Pattern Recognition*. Springer, 2013.

[42] E. Coumans and Y. Bai. Pybullet, a python module for physics simulation for games, robotics and machine learning, 2016–2021.

[43] B. Calli, A. Singh, J. Bruce, A. Walsman, K. Konolige, S. Srinivasa, P. Abbeel, and A. M. Dollar. Yale-cmu-berkeley dataset for robotic manipulation research. *The International Journal of Robotics Research*, 2017.

[44] O. Ronneberger, P. Fischer, and T. Brox. U-net: Convolutional networks for biomedical image segmentation. In *International Conference on Medical image computing and computer-assisted intervention*, 2015.